Mechanism of Nitrate Reduction by Desulfovio desulfuricans Nitrate Reductase - A Theoretical Investigation

Leopoldini, Monica; Russo, Nino; Toscano, Marirosa; Dulak, Marcin; Wesolowski, Tomasz Adam

CHEMISTRY
A EUROPEAN JOURNAL

DOI: 10.1002/chem.200500790

Mechanism of Nitrate Reduction by *Desulfovibrio desulfuricans* Nitrate Reductase—A Theoretical Investigation

Monica Leopoldini,[a] Nino Russo,*[a] Marirosa Toscano,[a] Marcin Dulak,[b] and Tomasz Adam Wesolowski[b]

Abstract: The oxidative half-reaction of oxygen atom transfer from nitrate to an Mo^{IV} complex has been investigated at various levels of theory. Two models have been used to simulate the enzyme active site. In the second, more advanced model, additional amino acid residues capable of significantly affecting the catalytic efficiency of the enzyme were included. B3LYP/6–31+G*, ONIOM, and orbital-free embedding approaches have been used to construct the potential energy profile and to qualitatively compare the results of a QM/MM study with those obtained by a full quantum mechanical strategy. The study has confirmed the utility of the orbital-free embedding method in the description of enzymatic processes.

Keywords: density functional calculations · enzyme models · nitrate reductase · ONIOM · orbital-free embedding

Introduction

The second-row transition-metal molybdenum is present in two classes of enzymes: the nitrogen-fixing nitrogenases, which possess an iron–molybdenum cofactor,[1] and mononuclear molybdenum enzymes (molybdoenzymes).[2] The latter catalyze oxygen atom transfer reactions to and from biological substrates in the nitrogen, sulfur, and carbon cycles.[3] According to their structures, molybdoenzymes can be further subdivided into three families: xanthine oxidases, sulfite oxidases, and dimethyl sulfoxide (DMSO) reductases.[2,4] Among the DMSO reductases are DMSO reductase itself, formate dehydrogenase (FDH), and periplasmatic nitrate reductase (NAP).[2] The cofactor in these enzymes is an organic pterin incorporating a dithiolene moiety, specifically bismolybdopterin guanine dinucleotide (MGD).[5]

Nitrate reductases play an important role in nitrogen assimilation, by catalyzing the reduction of nitrate to nitrite [Eq. (1)].[6]

$$NO_3^- + 2H^+ + 2e^- \rightarrow NO_2^- + H_2O \ (E'_0 = +420\,mV) \quad (1)$$

Recently, the first crystal structure of a dissimilatory (respiratory) nitrate reductase, at 1.9 Å resolution, has been determined by multi-wavelength anomalous diffraction (MAD) methods.[7] The enzyme is a monomeric polypeptide of the α/β-fold type, with a molecular mass of 80 kDa, and has a specific activity of 18.6 $U\,mg^{-1}$. The molecule is divided into four domains, each of which is involved in cofactor binding, but only one domain is responsible for the binding with an Fe_4S_4 cluster that serves as an electron pump.[7] Two MGD cofactors are embedded in the molecule and are stabilized by several hydrogen bonds with amino acid residues.[7] The Mo^{VI} is hexacoordinated with a distorted trigonal-prismatic geometry. The ligands comprise the four sulfur atoms of the dithiolene moieties, at an average distance of 2.3 Å from the Mo center, the sulfur atom of the side chain Cys140 residue (Mo–S bond length 2.5 Å), and a hydroxo/water molecule that completes the coordination sphere of the metal.

Access to the molybdenum center is facilitated by the presence of some charged residues, such as Arg354 and Asp155 which form a salt bridge, as well as Glu156 and Asp355. Hydrophobic residues towards the surface of the catalytic site cavity are Ala142, Val145, Val149, Leu359, and Leu362. Arg354 has been recognized as the anchoring site

[a] Dr. M. Leopoldini, Prof. N. Russo, Prof. M. Toscano
Dipartimento di Chimica and Centro di Calcolo ad Alte Prestazioni per Elaborazioni Parallele e Distribuite
Centro d'Eccellenza MIUR, Università della Calabria
87030 Arcavacata di Rende (CS) (Italy)
E-mail: nrusso@unical.it

[b] Dr. M. Dulak, Dr. T. A. Wesolowski
Université de Genève, Département de Chimie Physique
30, quai Ernest-Ansermet, 1211 Genève 4 (Switzerland)

for the negatively charged nitrate.[7] Conserved residues among all nitrate reductases are Gln346, Met308 (also found in FDH enzymes), and Met141.[7]

In the absence of crystallographic data on the reduced Mo^{IV} nitrate reductase form, Dias et al.[7] suggested a catalytic mechanism based on the behavior of the oxidized form, and on previous information concerning related enzymes and biomimetic model systems.[8–15]

In nitrate reductase, reaction starts with five-coordinate Mo^{IV} [$Mo^{IV}S^{Cys}(SR)_4$] (see the catalytic cycle in Scheme 1), which, in this oxidation state, can coordinate a nitrate ion. The latter binds to the metal center through one of its oxygen atoms, leading to a weakening of the relevant N–O bond. The Mo^{IV} is oxidized to Mo^{VI}, and NO_2^- is released.

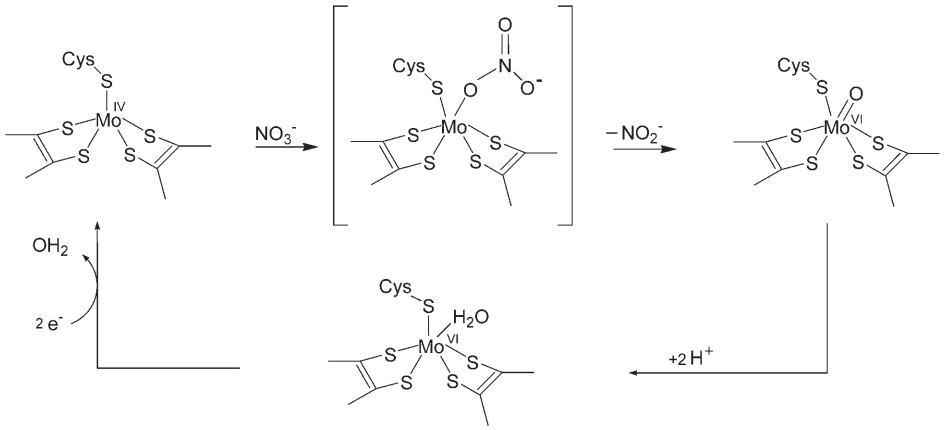

Scheme 1. Nitrate reductase catalytic mechanism.

Mo^{IV} is restored in another step, in which two protons are provided by water molecules present in the active site, and two electrons are provided by the Fe_4S_4 cluster.

Several computational studies[16–23] have been carried out on molybdoenzymes, employing model systems for the active sites. For example, it has been shown that sulfite oxidation by sulfite oxidase enzymes, which can be viewed as a reverse reaction of nitrate reduction, proceeds through attack of the lone pair of electrons of the sulfur atom on one of the oxo ligands at the molybdenum.[16] Other computational studies of phosphine oxidation[17,18] have led to similar results. Two DFT investigations concerning DMSO reductase[24,25] and trimethylamine *N*-oxide reductase[25] have been published, in which model systems of the general form $Mo^{IV}OR(S_2C_2R'_2)_2$ were used. Both of these studies showed the relevant reactions to occur through an associative mechanism involving the initial formation of a molybdenum-bound oxygen complex, transfer of the oxygen atom from the substrate to the metal center in which then leads to the products.

In this work, the oxidative half-reaction for oxygen atom transfer from nitrate to an Mo^{IV} complex has been investigated at various levels of theory. Two models were used to simulate the enzyme active site. The first model (A in Figure 1) was the bis(dimethyl dithiolene) structure, as used elsewhere[24] in a computational study on DMSO reductase that provided insight into the elementary steps of the oxo-transfer mechanism through the identification of all possible intermediates and transition states. The second model (B in Figure 1) was built up by supplementing the simpler model A with four nearby amino acid residues that are usually conserved within the family of nitrate reductases and formate dehydrogenases.[7]

Method and Computational Details

The coordinates of the protein were taken from the 1.9 Å resolution X-ray structure of *Desulfovibrio desulfuricans* nitrate reductase (PDB code = 2NAP).[7] Model A for the active site consists of an Mo^{IV} bis(dimethyl dithiolene) complex, in which the ligands represent a portion of the cofactor. An SCH_3 group chosen to mimic the Cys140 residue completes the metal ion coordination sphere.

Computations on this model were carried out using B3LYP/6–31+G*[26–31] and PW91PW91/6–31+G*[32–36] density functional protocols with the GAUSSIAN 03 code.[37] The LANL2DZ pseudopotential[38] for the metal ion was chosen in both sets of calculations. Singlet and triplet

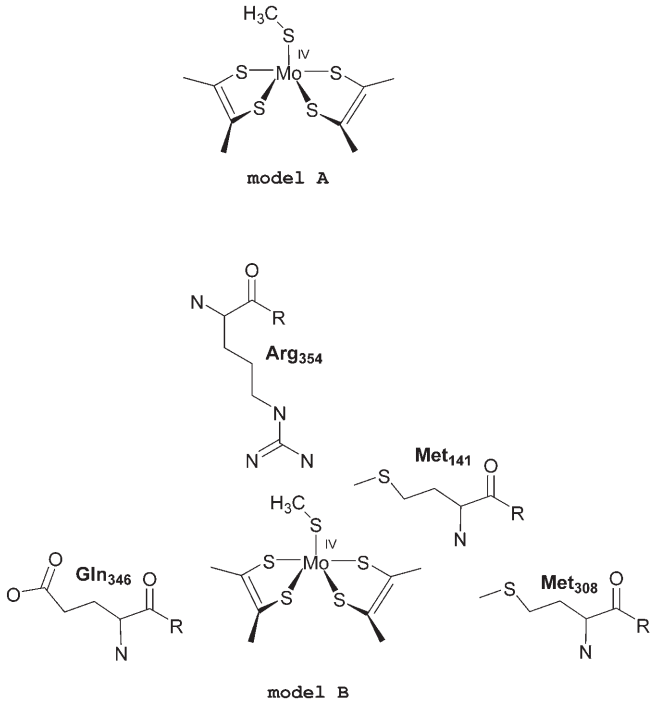

Figure 1. Structures of the models employed for the nitrate reductase active site. For both models, only a portion of the cofactor is used.

energy profiles were examined using restricted closed-shell and unrestricted open-shell approaches, respectively. No spin contamination was found for the triplet species, as evidenced by the fact that the value of $\langle S^2 \rangle$ was about 2 in all cases, with the value of 2.001 representing the greatest deviation from the ideal one.

Geometry optimization, performed at the B3LYP/6–31+G* level, was followed by vibrational analysis on all stationary points, to evaluate their character as minima or saddle points, and to compute zero-point energy (ZPE) corrections. The stability of each optimized triplet-state structure was checked by means of the Stable[39–41] procedure implemented in G03 code. Additional single-point calculations were performed with the PW91 PW91 functional.

Solvent effects were computed at the B3LYP level in the framework of the self-consistent reaction field polarized continuum model (SCRF-PCM)[42–44] using the UAHF[45] set of solvation radii to build the cavity for the solute in the gas-phase equilibrium geometries. A dielectric constant of $\varepsilon = 4$ was chosen to describe the protein environment of the active site in accordance with previous suggestions.[46,47]

Arg354, Met141, Met308, and Gln346, which are conserved residues in all nitrate reductase and formate dehydrogenase enzymes, were added to model A according to their crystallographic positions so as to obtain the more advanced model B. ONIOM and orbital-free embedding computations were performed on the latter model.

ONIOM methods have been extensively used[48–54] to compute potential energy profiles for large biological systems and have thereby yielded reliable information about the influence of the protein environment on active site structures and reaction energetics. To apply the ONIOM procedure, the system described by model B was divided into two parts, an inner and an outer layer. The inner layer consisted of the Mo^{IV} thiomethyl bis(dithiolene) complex, the nitrate substrate, and the nitrite product. The outer layer was made up of the amino acids Arg354, Met141, Met308, and Gln346, fixed in their crystallographic positions to prevent the optimization from giving an unrealistic expansion of the protein.[55] Hydrogen atoms were used to saturate fragments from the Protein Data Bank (PDB) structure, so as to avoid chemical artifacts. According to ONIOM terminology, the full system treated at a low level of theory is referred to as "real", while the inner layer is referred to as "model" and is treated at both low and high levels of theory.

The total energy E^{ONIOM} is defined according to Equation (2), where E(high, model) is the energy of the inner layer at the high level, E(low, real) is the energy of the total system at the low level, and E(low, model) is the energy of the inner layer obtained at the low level of theory.

$$E^{\mathrm{ONIOM}} = E(\text{high, model}) + E(\text{low, real}) - E(\text{low, model}) \quad (2)$$

For the two-layered ONIOM study, the B3LYP/6–31+G* and molecular mechanics UFF force field[56] approaches were used to perform high-level and low-level inner-layer calculations, respectively. The LANL2DZ pseudopotential was again used for the molybdenum ion.

Since the reliability of hybrid QM/MM methods depends on the parameters and calibration used, the orbital-free embedding approach[57] was also used to obtain a description that is not subject to these effects. Literature reports[58] have demonstrated the satisfactory performance of this method when applied to the modeling of metal-catalyzed reactions.

The ground-state electron density of an embedded system (atom, ion, molecule, or other polyatomic system) in a given environment can be derived from one-electron equations,[57] such as Equation (3) (atomic units are applied in all equations throughout the text), where ρ_A is the electron density of the embedded system constructed using one-electron functions ($\rho_A = 2\sum_{i=1}^{N} \phi_i^{\mathrm{KSCED}*}(\vec{r})\phi_i^{\mathrm{KSCED}}(\vec{r})$) and ρ_B is the electron density of the environment.

$$\left[-\tfrac{1}{2}\nabla^2 + V_{\mathrm{eff}}^{\mathrm{KSCED}}[\rho_A,\rho_B](\vec{r})\right]\phi_i^{\mathrm{KSCED}}(\vec{r}) = \varepsilon_i^{\mathrm{KSCED}}\phi_i^{\mathrm{KSCED}}(\vec{r}) \quad (3)$$

In these equations, $\rho_B(r)$ is a given function that can be derived either 1) from an equation coupled to Equation (3), in which the subsystems exchange their roles, or 2) by simpler methods (in particular, when it is to be kept constant in the process under investigation). In the second case, Equation (3) provides an embedding formalism based on first principles similar in spirit to commonly used empirical QM/MM techniques in simulations of biomolecules.[59] Since we were interested in the electronic structure of a metal-containing part of the active center ($\rho_A(r)$), we used a simpler method to derive $\rho_B(r)$ in this work. The superscript KSCED (Kohn–Sham Equations with Constrained Electron Density) is used to indicate that such quantities as the effective potential, orbitals, and orbital energies differ from the corresponding ones in the commonly used Kohn–Sham[60] equation [Eq. (4)], where $\rho = 2\sum_{i=1}^{N} \phi_i^{\mathrm{KS}*}(\vec{r})\phi_i^{\mathrm{KS}}(\vec{r})$.

$$\left[-\tfrac{1}{2}\nabla^2 + V_{\mathrm{eff}}^{\mathrm{KS}}[\rho](\vec{r})\right]\phi_i^{\mathrm{KS}}(\vec{r}) = \varepsilon_i^{\mathrm{KS}}\phi_i^{\mathrm{KS}}(\vec{r}) \quad (4)$$

The effective potential in Equation (3) differs from that in Equation (4) by additional terms describing the interactions between the two subsystems. These terms have a universal system-independent form,[57] [Eq. (5)], where N_B is the number of nuclei in subsystem B, and Z_α^B is the nuclear charge of nucleus α in subsystem B:

$$V_{\mathrm{eff}}^{\mathrm{emb}(KSCED)}[\rho_A,\rho_B](\vec{r}) = -\sum_{\alpha}^{N_B}\frac{Z_{\alpha}^{\mathrm{B}}}{|\vec{R}_{\alpha}^{\mathrm{B}}-\vec{r}|} + \int\frac{\rho_B(\vec{r}\prime)}{|\vec{r}-\vec{r}'|}dr' + \frac{\delta E_{xc}[\rho]}{\delta\rho}|_{\rho=\rho A+\rho B} - \frac{\delta E_{xc}[\rho]}{\delta\rho}|_{\rho=\rho A} + -\frac{\delta T_{\mathrm{S}}^{\mathrm{nad}}[\rho_1,\rho_2]}{\delta\rho_1}|_{\rho 1=\rho A} \quad (5)$$

The exchange-correlation functional $E_{xc}[\rho]$ is defined as in the Kohn–Sham formalism,[60] and the non-additive kinetic energy $T_{\mathrm{S}}^{\mathrm{nad}}[\rho_1,\rho_2]$, a functional depending on two electron densities, is defined by Equation (6), where $T_s[\rho]$ is the kinetic energy of the reference system of the non-interacting electrons.

$$T_{\mathrm{S}}^{\mathrm{nad}}[\rho_1,\rho_2] = T_s[\rho_1+\rho_2]-T_s[\rho_1]-T_s[\rho_2] \quad (6)$$

Equations (3) and (4) have different solutions, which depend on the environment represented in the KSCED embedding potential through the positions and electric charges of atomic nuclei and the electron density of the environment. In the case of a constant ρ_B, as applied in this work, calculation of the environment-induced changes in the electronic structure of the investigated subsystem follows a simple strategy: the shift of a calculable observable is obtained as the difference between the values derived from Equation (3) for the embedded subsystem A and Equation (4) for the isolated subsystem A.

Practical application of the outlined strategy, however, involves several challenging issues and has the following requirements: 1) availability of good approximations to the density functionals of unknown analytical form (all but the first two terms on the right-hand-side of Equation (5)), 2) an efficient computer implementation of Equations (3)–(5), allowing for fast evaluation of embedded orbitals and observables of interest, and 3) a computationally efficient way of obtaining the electron density of the environment ρ_B. As far as the first requirement is concerned, we use a system-independent approximation of the kinetic-energy-dependent component of the embedding potential applicable in such cases where the ρ_A,ρ_B overlap is small.[61] This approximation, denoted as GGA97 herein, uses a generalized gradient approximation of $T_s[\rho]$ in Equation (6), in which the gradient dependency has the same analytical form as that of the PW91 exchange functional,[33] with the coefficients adopted for the kinetic energy by Lembarki and Chermette.[62] Therefore, applications of the orbital-free embedding formalism are currently limited to cases of small ρ_A,ρ_B overlap. The absence of covalent bonding between subsystems *A* and *B* can be used as a practical rule of thumb for applicability of these approximations.

We used an efficient computer implementation of the orbital-free embedding deMon2 K-KSCED,[63] based on use of the code deMon2 K[64] to solve Kohn–Sham equations [Eq. (4)].

The PW91 PW91 exchange-correlation functional was used for both Kohn–Sham and KSCED calculations. The DZVP basis set[65] and automatically generated auxiliary GEN-A2* functions[66] were used.

Results and Discussion

Isolated gas-phase reaction (model A): It was suggested that the oxo-transfer reaction, mediated by molybdenum(IV) bis-(dithiolene) complexes, such as $[M^{IV}(O\text{-}p\text{-}C_6H_4X)(S_2C_2Me_2)_2]^-$, follows second-order kinetics with an associative transition state characterized by a large negative activation entropy.[67] The proposed transition state involves the main feature of M–OX bond-making with concomitant X–O bond-weakening. The mediatory complexes have square-pyramidal structures, which are converted to distorted *cis*-octahedral structures upon oxidation. Transition states are expected to resemble the distorted *cis*-octahedral configurations.[67]

The B3LYP-optimized geometry for molybdenum(IV) model system A in its singlet electronic state was found to be square pyramidal, with average Mo–S(dithiolene) distances of 2.365 Å and an Mo–S^{Cys} bond length of 2.347 Å. Our structure agrees very well with experimental structures determined by Holm and co-workers for phenoxy complexes,[68] except for the axial bond, which in our case is longer because of the greater atomic radius of sulfur compared to that of oxygen. Furthermore, the same orientation was found for the recently published computational model $[Mo(OCH_3)(S_2C_2Me_2)_2]^{1-}$.[24,25]

Interestingly, another low-energy structure for this complex was localized at the B3LYP level, arising from a triplet electronic state. It shows an essentially distorted trigonal-bipyramidal arrangement, in which dithiolene sulfur atoms occupy both equatorial and axial positions (mean equatorial Mo–S distance 2.465 Å, mean axial Mo–S distance 2.365 Å). The energy gap between the B3LYP low-spin and high-spin states is only 4.7 kcal mol^{-1}, the singlet state being the ground state.

The triplet state was not observed experimentally for molybdenum(IV) bis(dithiolene) mimics of the active site of molybdoenzymes, and there are no experimental data concerning singlet–triplet energy splitting in these compounds. Experimental studies on molybdoenzymes suggested a diamagnetic state for both Mo^{IV} and Mo^{VI}.[69] A recent photoelectron spectroscopy study on the $[Mo^{IV}O(mnt)_2]^{2-}$ complex indicated the singlet configuration as the ground state, although the triplet structure was not taken into account by the authors.[70]

Since the multiplicity of the species involved in the catalytic cycle is far from certain, we were interested in exploring the potential energy surfaces (PES) of both the singlet and triplet states. Both PES are sketched in Figure 2, which shows the relative energies of all the intermediates, transition states, and exit channels with respect to the ground-state asymptotes.

As suggested both experimentally[60] and theoretically,[24,25] the oxidative reaction starts with the formation of a stable

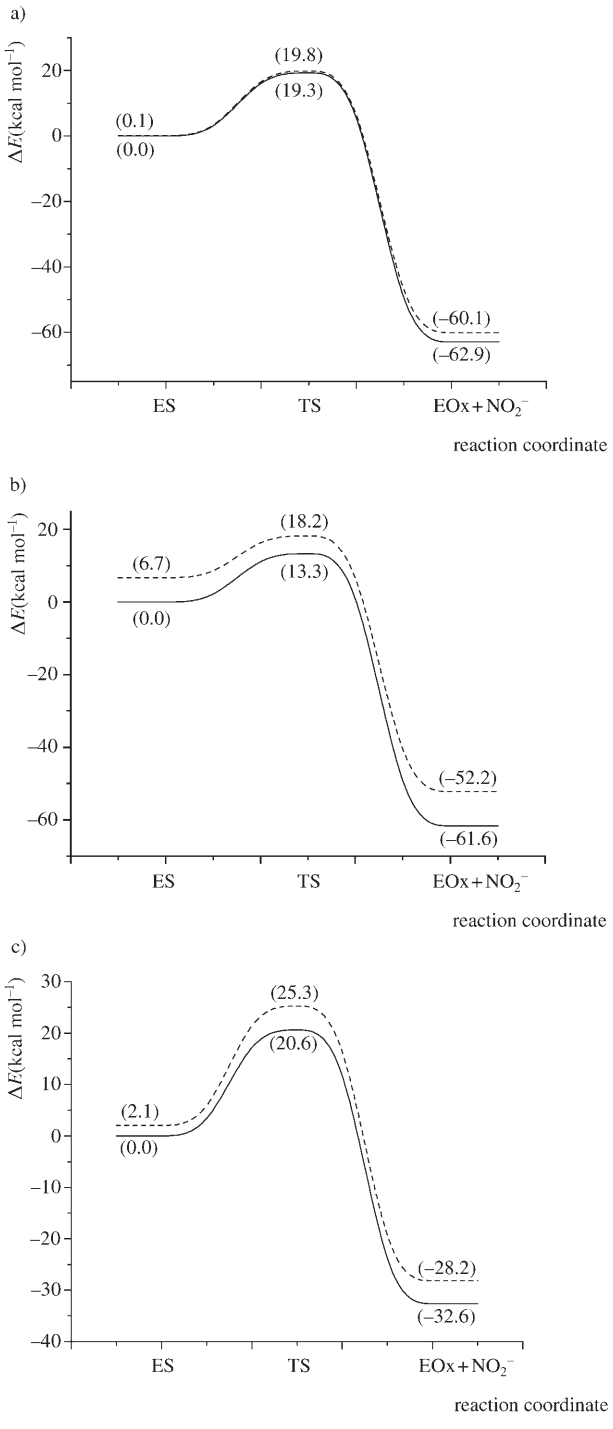

Figure 2. Potential energy surfaces calculated for model A at a) gas-phase B3LYP(B3LYP/6-31+G*/lanl2dz), b) PW91PW91 (PW91PW91/6-31+G*/lanl2dz), and c) solvated B3LYP levels (PCM(B3LYP/6-31+G*/lanl2dz)). Singlet: solid line; triplet: dashed line.

intermediate between the molybdenum complex and the substrate (ES in Figure 3a). The NO_3^- binds to the metal center through one of its oxygen atoms. In the case of the low-spin state, an interaction is established that results in an Mo–O(nitrate) distance of 2.270 Å. As a consequence of this interaction, the O–N bond length in the substrate

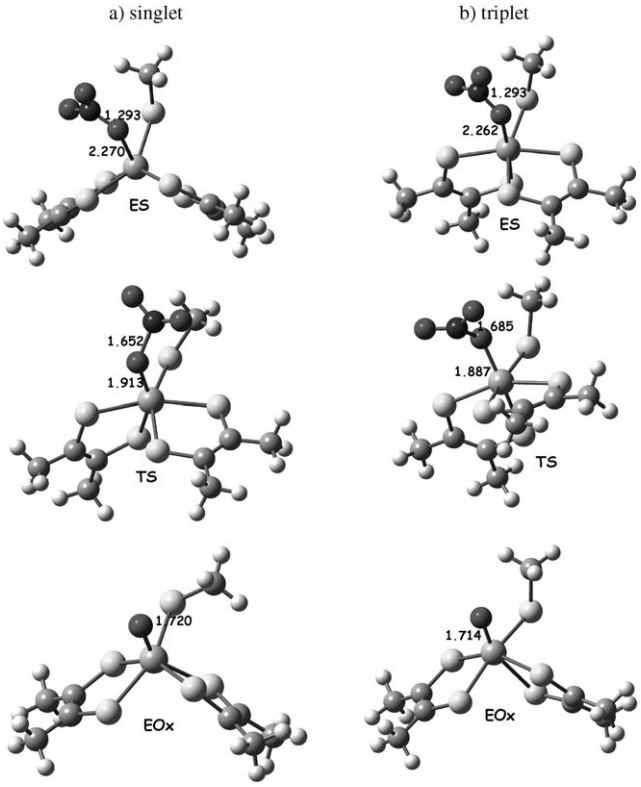

Figure 3. a) Singlet and b) triplet B3LYP-optimized geometries for ES, TS, and EOx points for model A.

lengthens from 1.265 to 1.293 Å. The coordination geometry around the molybdenum becomes trigonal prismatic, with all the Mo–S(dithiolene) distances falling in the range 2.406–2.459 Å and an Mo–S^{Cys} bond length of 2.433 Å. In their respective studies on DMSO reductase mimics, Hall[24] and Thapper[25] obtained very similar geometries for the enzyme–substrate complex.

For the triplet state, the optimized equilibrium geometry is close to a distorted octahedral structure (Figure 3b). Nitrate occupies one axial position and the Mo–O(nitrate) distance is 2.262 Å. The other axial position is occupied by a dithiolene sulfur (Mo–S distance 2.433 Å; S-Mo-O(nitrate) angle 175.6°). The remaining dithiolene sulfur atoms occupy equatorial positions at distances of 2.435, 2.500, and 2.527 Å from the molybdenum. S^{Cys} occupies the final equatorial position, with the methyl group pointing towards the nitrate ligand (Mo–S^{Cys} distance 2.476 Å). The singlet–triplet splitting pertaining to this intermediate is only 0.1 kcal mol^{-1}, with the low-spin state again being the ground state.

The oxo-transfer reaction passes through a transition state having respective Mo–O(nitrate) and O(nitrate)–N(nitrate) distances of 1.913 and 1.652 Å for the singlet spin state and 1.887 and 1.685 Å for the triplet spin state. As can be seen in Figure 3, the ligand arrangements in the low-spin and high-spin transition states appear to be very distorted with respect to the ideal trigonal-prismatic and octahedral geometries. The imaginary frequencies of 589 cm^{-1} for the singlet state (IR intensity 232 km mol^{-1}) and 722 cm^{-1} for the

triplet state (IR intensity 297 km mol^{-1}), which confirm the saddle-point character of these two stationary points, correspond to the stretching vibration modes of the Mo–O(nitrate) and O(nitrate)–N(nitrate) bonds. The low-spin and high-spin transition states are substantially degenerate. Taking the ground state of the enzyme–substrate complex as a reference, the singlet and triplet transition states lie at 19.3 and 19.8 kcal mol^{-1}, respectively.

After N–O bond-breaking, the reaction proceeds towards the formation of the oxo Mo^{VI} complex and the NO_2^- product. The $[Mo^{VI}O(SCH_3)(S_2C_2Me_2)_2]^{1-}$ species (EOx in Figure 3a,b) exhibit distorted geometries. The Mo–O bond lengths are 1.720 Å and 1.714 Å for the singlet and triplet states, respectively. Products are found at 62.9 kcal mol^{-1} (low-spin) and 60.1 kcal mol^{-1} (high-spin) below the reference. As can be noted from Figure 2, the low-spin state is lower in energy with respect to the high-spin one, with the energetic gap between them increasing slightly on going from reactants to products.

The effect of a better representation of the MGD portion, which we realized by using a model for the cofactor in which the guanidine and phosphate groups were neglected, did not introduce significant variation in the gaps between the various species encountered along the respective singlet and triplet potential energy profiles. The only exception was the energy separation between the products in their different electronic states, which became 4.5 kcal mol^{-1} larger.

Our results are in qualitative agreement with those of Hall and Webster[24] and Thapper et al.[25] for DMSO reductase, and with those suggested experimentally on the basis of a study of analogous molybdenum reaction systems.[68] The rate-limiting step is recognized as the electron-transfer step that occurs through the transfer of the oxygen atom from the bound substrate to the metal center. The relative barrier height in a DMSO reductase model system was found to be 8.9 kcal mol^{-1} at the B3LYP level[24] and 14.3 kcal mol^{-1} at the LDA level.[25] The barriers estimated in our study are higher than those proposed in this previous investigation. A simple explanation for this discrepancy may lie in the different strengths of the O–N bond in nitrate and the O–S bond in the DMSO molecule.

In the same paper, Thapper et al.[25] also reported an investigation, at LDA approximation level, of the reduction of Me_3NO by Me_3NO reductase, which possesses the same dithiolene active site structure as in the present study, but with an oxo ligand instead of an amino acid residue. The reduction of Me_3NO proceeds via a bound substrate intermediate, a transition state, and a product all described as distorted octahedral. The authors did not find the trigonal-prismatic arrangement found for DMSO reductase. Kaupp[71] suggested that hexacoordinate d^0 or d^2 systems (Mo^{VI} and Mo^{IV}, respectively) may prefer "non-VSEPR" structures when σ bonds are involved, whereas π bonding situations seem to favour octahedral metal coordination. At this stage, we would like to point out that the electronic configuration is likely to twist the coordination geometry towards the trigonal-prismatic limit. Table 1 lists the values of the main geometrical parameters for the reactant complexes,

Table 1. Selected geometrical parameters of optimized geometries for model A.

Parameter	ES		TS		EOx	
distances	singlet	triplet	singlet	triplet	singlet	triplet
Mo–SCH_3	2.433	2.476	2.488	2.534	2.558	2.529
S–CH_3	1.844	1.841	1.844	1.841	1.835	1.840
Mo–O(nitrate)	2.270	2.262	1.913	1.887	1.720	1.714
O(nitrate)–N(nitrate)	1.293	1.293	1.652	1.685	–	–
Mo–S_1	2.416	2.435	2.442	2.483	2.452	2.456
Mo–S_2	2.406	2.433	2.444	2.564	2.487	2.432
Mo–S_3	2.421	2.500	2.495	2.500	2.469	2.559
Mo–S_4	2.459	2.527	2.506	2.438	2.532	2.529
angles						
Mo-S-CH_3	112.4	108.4	111.2	104.9	98.7	105.2
Mo-O(nitrate)–N(nitrate)	129.1	132.5	135.1	129.5	–	–
O(nitrate)-Mo-SCH_3	82.9	89.0	94.0	85.0	88.6	90.0
S_1-Mo-S_2	80.4	82.5	80.8	79.0	78.9	82.2
S_3-Mo-S_4	80.0	79.7	78.0	81.5	77.9	76.5
S_1-Mo-S_3	88.2	90.2	158.5	97.0	82.2	82.4
S_2-Mo-S_4	80.8	91.2	100.7	85.2	72.2	81.9
O(nitrate)-Mo-S_2	129.1	175.6	150.7	162.9	143.9	158.9

transition states, and products for both multiplicities. In the singlet ES complex, the dithiolene moieties can be viewed as S=CR groups in both pterins (see the M–S distances in Table 1), representing poor π-donor ligands (trigonal prism). The optimized geometry for the high-spin complex, however, suggests one pterin with two S=CR groups, and the other one as a dianionic dithiolate. In fact, the Mo–S bond lengths listed in Table 1 are different in the two pterin ligands. This last situation gives rise to single-sided π donors (octahedral coordination). The O(nitrate)-Mo-S_2 angle may be viewed as a measure of this twisting. In the low-spin ES complex it has a value of 129.1°, while in the case of the high-spin complex it has a value of 175.6°, nearer the ideal octahedral value of 180°.

The involvement of two spin states in oxo-transfer reactions catalyzed by systems analogous to molybdoenzymes has never been postulated previously, and no theoretical information is available for comparison. The only theoretical data concerning the energetic order of the singlet and triplet states in molybdenum complexes can be found in a DFT study[72] carried out on 16-electron $[d^4\text{-}\eta^5\text{-}CpMo(CO)_2X]$ complexes. The singlet–triplet gap seemed to depend on the method or exchange correlation functional employed, with DFT/BPW91, CCSD(T), and CASSCF exaggerating the gap with respect to the hybrid DFT/B3LYP approach.

For this reason, we repeated our computation using the gradient-corrected PW91PW91 functional. The potential energy profile obtained with PW91PW91 on B3LYP-optimized geometries is depicted in Figure 2b.

Both functionals favor the singlet state, but PW91PW91 enhances the gap between the spin states. It is worth noting that the barrier also becomes lower, especially in the case of the singlet PES. As suggested by some literature data,[73–75] this may be due to the fact that the PWnPW91 functionals, as opposed to the B3LYP one, describe long-range interactions in a different way.

In the high-spin case, products are located 9.5 kcal mol^{-1} above the same species in the low-spin state. In the minimum-energy path, both the B3LYP and PW91PW91 functionals predict similar exothermicities.

B3LYP single-point evaluation of solvation energy (values are reported in Figure 2c) shows that some effect occurs due to the protein environment described by the continuum dielectric constant of 4. A slight increase in the low-spin/high-spin gap occurs at the ES point (the singlet lies 2.1 kcal mol^{-1} below the triplet). Transition states are found at 20.6 kcal mol^{-1} (singlet) and 25.3 kcal mol^{-1} (triplet) with respect to the ES point, underlining the fact that the triplet is to some extent destabilized with respect to the singlet by the protein environment. The overall reaction is less exothermic compared to that in the gas phase, since EOx + NO_2^- products lie 32.6 kcal mol^{-1} (singlet) and 28.2 kcal mol^{-1} (triplet) below the reference ES species.

The reason for which the reaction in solvent becomes less favoured from a thermodynamic point of view lies in the fact that the solvation, on going from ES to separated products, concerns species of different charge. The different polarizations induced by these solutes on the solvent precludes comparison of this result with that obtained in the gas phase.

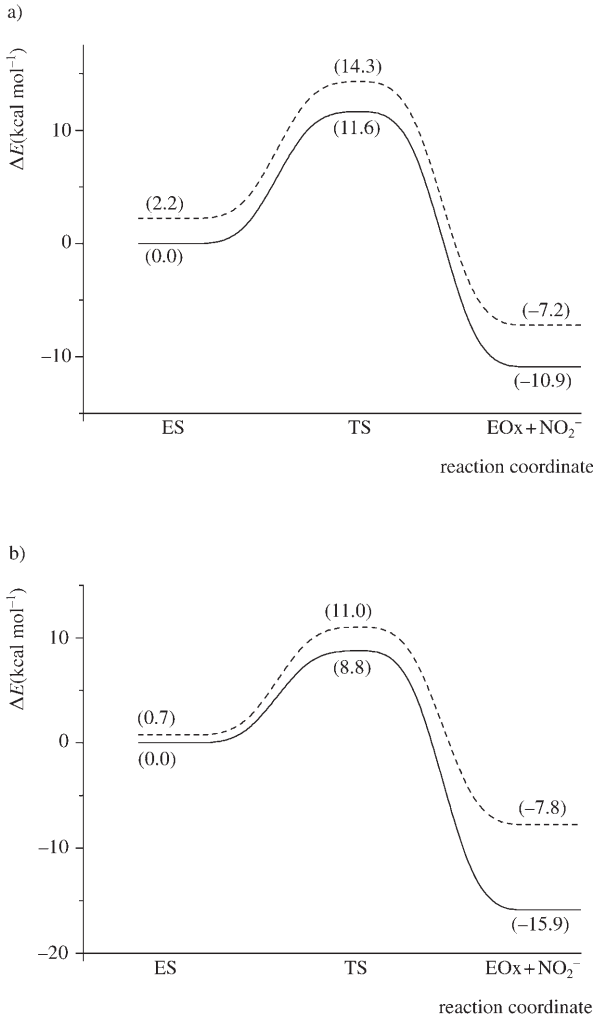

Figure 4. a) ONIOM(B3LYP:UFF) and b) orbital-free embedding potential energy surfaces calculated for model B. Singlet: solid line; triplet: dashed line.

Protein environment (model B): Model A was supplemented with the amino acids Arg354, Met141, Met308, and Gln346 to build up model B. The aim here was to evaluate the influence and the role of the environment on the overall oxo-transfer reaction.

The ONIOM energetic profiles for both singlet and triplet states of the enzyme are depicted in Figure 4a. Optimized geometries of the structures involved in the reaction sequence of Scheme 1 and corresponding to the stationary points on the reaction path are given in Figure 5.

The nitrate-bound Mo^{IV} low-spin complex (ES in Figure 5a) is characterized by an interaction between the metal and the substrate oxygen atom that is stronger than that in the case of the analogous complex with model A. In fact, the Mo–O(nitrate) and O(nitrate)–N(nitrate) distances are 2.183 Å and 1.378 Å, respectively, underlining the fact that nitrate is already activated for the reduction process. The trigonal-prismatic geometry around the molybdenum appears to be much more distorted than in model A. In the high-spin adduct, the nitrate interacts with the molybdenum at a distance of 2.147 Å. As a consequence, the O(nitrate)–N(nitrate) distance in the substrate becomes 1.389 Å. The complex assumes a distorted octahedral geometry, with nitrate and one pterin sulfur in the axial positions and the remaining ligands in the equatorial positions. Contrary to what was presumed, but not corroborated by objective data, by Dias et al.,[7] our computations indicate that there is no interaction between the metal-bound nitrate molecule and the Arg354 residue. This led us to think that the supposed anchoring of nitrate by means of the positive charge of Arg354[7] could occur in a preliminary phase of the catalytic cycle.

The singlet and triplet ES evolve into products through transition states (TS). The transition state for the singlet species has Mo–O(nitrate) and O(nitrate)–N(nitrate) distances of 1.859 Å and 1.782 Å, respectively. Its structure can be described as a trigonal prism like that obtained in the calculations on model A. The imaginary frequency at 252 cm^{-1} corresponds to the stretching of the Mo–O(nitrate) and O(nitrate)–N(nitrate) bonds.

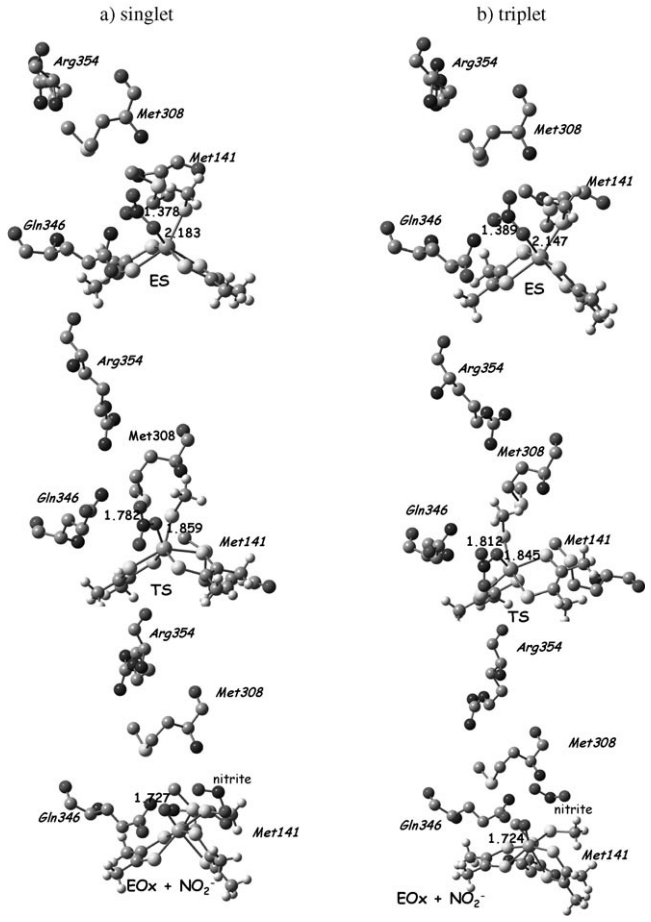

Figure 5. a) Singlet and b) triplet ONIOM(B3LYP:UFF)-optimized geometries for ES, TS, and EOx + NO_2^- points for model B.

For the triplet, the transition state is characterized by Mo–O(nitrate) and O(nitrate)–N(nitrate) distances of 1.845 Å and 1.812 Å, respectively, and the imaginary frequency at 444 cm^{-1} corresponds to the same vibrational mode as that of the singlet. The metal ion shows a distorted octahedral coordination, with an S^{Cys}-Mo-S_4 angle of 109.7°, that is, markedly different from the octahedral value.

After this transition state is reached, the reaction proceeds to yield the Mo^{VI} oxo complex EOx along with the nitrite molecule. The low-spin and high-spin products share octahedral coordination geometry about the molybdenum, with the oxo ligand occupying an axial position. The Mo–O(nitrate) distances in the low-spin and high-spin complexes are 1.727 and 1.724 Å, respectively. In the ONIOM description, the product also contains a nitrite ion that remains at a distance of 4.233 Å (singlet) or 3.046 Å (triplet) from the metal-bound oxygen atom. In the case of computations on model A, it was impossible to obtain geometry convergence in the presence of a long-range interaction between nitrite and the oxomolybdenum(VI) complex. The energy value of the product in the latter case thus corresponds to a summation of the energy values of the infinitely separated products (E(EOx) + $E(NO_2^-)$). This means that the energetics obtained with model A and with model B cannot be compared at product level.

The E^{ONIOM} gap between the singlet and triplet ES is 2.2 kcal mol^{-1}, the singlet state being the ground state. As is clear from a comparison of the data in Figure 2a with those in Figure 4a, this gap is influenced by the presence of the protein environment.

Transition states are found at 11.6 kcal mol^{-1} and 14.3 kcal mol^{-1} above the ES starting point for the singlet and triplet, respectively. The barrier for the oxo transfer appears to be significantly reduced by the presence of the amino acids. The products are found at 10.9 kcal mol^{-1} and 7.2 kcal mol^{-1} below the energy of the ES complex for the low-spin and high-spin cases, respectively.

The protein environment seems not to influence the mechanism of nitrate reduction. The overall reaction involves the formation of a substrate-metal complex and a transition state with Mo–ONO_2^- bond-forming character, after which the oxygen atom is fully transferred to the metal center. However, the nearby amino acids accelerate the process by lowering the activation energies. This feature depends on the influence of the protein environment in making the active site slightly strained. This strain is crucial for the reactivity, as pointed out by Morokuma et al.,[55] because it acts as a device for the accumulation of energy, which can be used in later steps of the catalytic cycle to overcome barriers. This entatic principle has also been proposed by Hall and Webster[24] for the reaction of DMSO reductase.

It is worth noting that the effect of the protein environment described by the ONIOM procedure is qualitatively comparable to that obtained using the PCM approach on model A. In fact, both methods suggest a lower exothermicity of the reaction with respect to that in the gas phase.

Orbital-free embedding reaction model B: The ONIOM procedure allowed us to evaluate the effect of the protein environment on the catalytic efficiency of the enzyme using a low level of theory represented by a molecular mechanics approach. More reliability can be expected if the surrounding amino acids are treated quantum mechanically, confining the SCF calculations to a relatively small subsystem and keeping the electron density of the rest of enzyme frozen. Thus, using the equilibrium geometries obtained at ONIOM(B3LYP:UFF) level, an orbital-free embedding analysis was carried out on this type of system for the first time. Single-point evaluation was performed using the PW91PW91 exchange-correlation- and GGA97 non-additive kinetic energy functionals. At the moment, KSCED formalism has two tested levels of approximation, namely LDA and GGA. We employed the GGA level because of its statistically better accuracy. This introduces more than one variable that one needs to consider in an eventual comparison with the ONIOM data set (i.e., methodology, functional, and basis set); thus, we will consider only the qualitative aspects of these results.

The orbital-free embedding potential energy profiles are depicted in Figure 4b, showing the relative energies for both the singlet and triplet species. The results show that the singlet-triplet gap increases on going from ES to TS to EOx. The ES singlet species is the ground state and it lies 0.7 kcal mol^{-1} below the triplet state.

The oxo transfer requires an activation energy of 8.8 kcal mol^{-1} for the low-spin and 11.0 kcal mol^{-1} for the high-spin system. At this point of the reaction, the singlet-triplet splitting is only 2.2 kcal mol^{-1}. The products are found at 7.8 kcal mol^{-1} (singlet) and 15.9 kcal mol^{-1} (triplet) below the singlet ES complex.

As can be noted, notwithstanding the aforementioned differences in the methodologies used, the general information that one can obtain from the analysis of orbital-free embedding data is very similar to that obtained with the other methods, but offers the guarantee of a totally quantum-mechanical treatment.

Conclusions

The mechanism of nitrate reduction by *Desulfovibrio desulfuricans* nitrate reductase has been investigated by means of quantum-mechanical and QM/MM methods. On the basis of the results obtained, we can draw the following conclusions:

All computations indicate that the enzymatic process involves the formation of an $[Mo^{IV}(SCH_3)(NO_3)(S_2C_2Me_2)_2]^{2-}$ complex, which, through a transition state characterized by the breaking of an N–O and the formation of an Mo–O bond, evolves towards NO_2^- and $[Mo^{VI}O(SCH_3)(S_2C_2Me_2)_2]^{1-}$ as products. Both singlet and triplet electronic states can, in principle, be involved in the catalytic event, although the low-spin state represents the ground state for all stationary points on the potential-energy surface.

The most significant differences between the three examined descriptions seem not to depend on the computational tool, but rather on the choice of model used to simulate the active site of the enzyme. In particular, the height of the activation barrier is significantly affected by the presence of nearby amino acid residues, which induce a certain strain in the catalytic core, thereby enhancing its reactivity.

From a quantitative point of view, the relevant barrier was computed not to be significantly different at the ONIOM(B3LYP:UFF) and orbital-free embedding levels of theory.

This study represents the first tentative attempt to apply the concept of frozen surrounding density to obtain a spin-dependent potential energy surface for an enzyme-catalyzed reaction.

Acknowledgements

We gratefully acknowledge the Università della Calabria and the POR Regione Calabria for financial support. This research was also supported by grants from the Swiss National Science Foundation.

[1] B. K. Burgess, D. J. Lowe, *Chem. Rev.* **1996**, *96*, 2983.
[2] R. Hille, *Chem. Rev.* **1996**, *96*, 2757.
[3] A. Thapper, C. Lorber, J. Fryxelius, A. Behrens, E. Nordlander, *J. Inorg. Biochem.* **2000**, *79*, 67.
[4] R. Hille, *J. Biol. Inorg. Chem.* **1996**, *1*, 397.
[5] D. Collison, C. D. Garner, J. A. Juole, *Chem. Soc. Rev.* **1996**, *21*, 25.
[6] J. A. Craig, R. H. Holm, *J. Am. Chem. Soc.* **1989**, *111*, 2111.
[7] M. J. Dias, M. E. Than, A. Humm, R. Huber, G. P. Bourenkov, H. D. Bartunik, S. Bursakov, J. Calvete, J. Caldeira, C. Carneiro, J. J. G. Moura, I. Moura, M. J. Romao, *Structure* **1999**, *7*, 65.
[8] R. A. D. Wentworth, *Coord. Chem. Rev.* **1976**, *18*, 1.
[9] S. P. Cramer, L. P. Solomonson, W. W. W. Adams, R. E. Mortenson, *J. Am. Chem. Soc.* **1984**, *106*, 1467.
[10] R. Hille, *Chem. Rev.* **1987**, *87*, 1401.
[11] J. C. Boyington, V. N. Gladyshev, S. V. Khangulov, T. C. Stadtman, P. D. Sun, *Science* **1997**, *275*, 1305.
[12] B. S. Lim, R. H. Holm, *J. Am. Chem. Soc.* **2001**, *123*, 1920.
[13] K. M. Sung, R. H. Holm, *J. Am. Chem. Soc.* **2001**, *123*, 1931.
[14] K. M. Sung, R. H. Holm, *J. Am. Chem. Soc.* **2002**, *124*, 4312.
[15] B. S. Lim, K. M. Sung, R. H. Holm, *J. Am. Chem. Soc.* **2000**, *122*, 7410.
[16] A. Thapper, R. J. Deeth, E. Nordlander, *Inorg. Chem.* **1999**, *38*, 1015.
[17] M. R. Bray, Ph. D. Thesis, University of Warwick, Coventry, UK, **1997**.
[18] M. A. Pietsch, M. B. Hall, *Inorg. Chem.* **1996**, *35*, 1273.
[19] M. R. Bray, R. J. Deeth, *Inorg. Chem.* **1996**, *35*, 5720.
[20] M. R. Bray, R. J. Deeth, *J. Chem. Soc. Dalton Trans.* **1997**, 4005.
[21] P. Ilich, R. Hille, *J. Chem. Phys.* **1999**, *103*, 5406.
[22] M. R. Bray, R. J. Deeth, *J. Chem. Soc. Dalton Trans.* **1997**, 1267.
[23] a) A. A. Voityuk, K. Albert, S. Kostlmeier, V. A. Nasluzov, K. M. Neyman, P. Hof, M. J. Romao, N. Rosch, *J. Am. Chem. Soc.* **1997**, *119*, 3159; b) A. A. Voityuk, K. Albert, M. J. Romao, R. Huber, N. J. Rosch, *Inorg. Chem.* **1998**, *37*, 176.
[24] C. E. Webster, M. B. Hall, *J. Am. Chem. Soc.* **2001**, *123*, 5820.
[25] A. Thapper, R. J. Deeth, E. Nordlander, *Inorg. Chem.* **2002**, *41*, 6695.
[26] A. D. J. Becke, *Chem. Phys.* **1993**, *98*, 5648.
[27] C. Lee, W. Yang, R. G. Parr, *Phys. Rev. B* **1988**, *37*, 785.
[28] R. Ditchfield, W. J. Hehre, J. A. Pople, *J. Chem. Phys.* **1971**, *54*, 724.
[29] W. J. Hehre, R. Ditchfield, J. A. Pople, *J. Chem. Phys.* **1972**, *56*, 2257.
[30] P. C. Hariharan, J. A. Pople, *Mol. Phys.* **1974**, *27*, 209.
[31] M. S. Gordon, *Chem. Phys. Lett.* **1980**, *76*, 163.
[32] K. Burke, J. P. Perdew, Y. Wang in *Electronic Density Functional Theory: Recent Progress and New Directions* (Eds.: J. F. Dobson, G. Vignale, M. P. Das), Plenum, **1998**.
[33] J. P. Perdew in *Electronic Structure of Solids '91* (Eds.: P. Ziesche, H. Eschrig), Akademie Verlag, Berlin, **1991**, p. 11.
[34] J. P. Perdew, J. A. Chevary, S. H. Vosko, K. A. Jackson, M. R. Pederson, D. J. Singh, C. Fiolhais, *Phys. Rev. B* **1992**, *46*.
[35] J. P. Perdew, J. A. Chevary, S. H. Vosko, K. A. Jackson, M. R. Pederson, D. J. Singh, C. Fiolhais, *Phys. Rev. B* **1993**, *48*.
[36] J. P. Perdew, K. Burke, Y. Wang, *Phys. Rev. B* **1996**, *54*, 16533.
[37] GAUSSIAN 03, M. J. Frisch, G. W. Trucks, H. B. Schlegel, G. E. Scuseria, M. A. Robb, J. R. Cheeseman, J. A. Montgomery, Jr., T. Vreven, K. N. Kudin, J. C. Burant, J. M. Millam, S. S. Iyengar, J. Tomasi, V. Barone, B. Mennucci, M. Cossi, G. Scalmani, N. Rega, G. A. Petersson, H. Nakatsuji, M. Hada, M. Ehara, K. Toyota, R. Fukuda, J. Hasegawa, M. Ishida, T. Nakajima, Y. Honda, O. Kitao, H. Nakai, M. Klene, X. Li, J. E. Knox, H. P. Hratchian, J. B. Cross, C. Adamo, J. Jaramillo, R. Gomperts, R. E. Stratmann, O. Yazyev, A. J. Austin, R. Cammi, C. Pomelli, J. W. Ochterski, P. Y. Ayala, K. Morokuma, G. A. Voth, P. Salvador, J. J. Dannenberg, V. G. Zakrzewski, S. Dapprich, A. D. Daniels, M. C. Strain, O. Farkas, D. K. Malick, A. D. Rabuck, K. Raghavachari, J. B. Foresman, J. V. Ortiz, Q. Cui, A. G. Baboul, S. Clifford, J. Cioslowski, B. B. Stefanov, G. Liu, A. Liashenko, P. Piskorz, I. Komaromi, R. L. Martin, D. J. Fox,

T. Keith, M. A. Al-Laham, C. Y. Peng, A. Nanayakkara, M. Challacombe, P. M. W. Gill, B. Johnson, W. Chen, M. W. Wong, C. Gonzalez, J. A. Pople, Gaussian, Inc., Pittsburgh PA, **2003**.
[38] P. J. Hay, W. R. Wadt, *J. Chem. Phys.* **1985**, *82*, 270; P. J. Hay, W. R. Wadt, *J. Chem. Phys.* **1985**, *82*, 284; P. J. Hay, W. R. Wadt, *J. Chem. Phys.* **1985**, *82*, 299.
[39] R. Seeger, J. A. Pople, *J. Chem. Phys.* **1977**, *66*, 3045.
[40] R. Bauernschmitt, R. Ahlrichs, *J. Chem. Phys.* **1996**, *104*, 9047.
[41] H. B. Schlegel, J. J. McDouall in *Computational Advances in Organic Chemistry* (Eds.: C. Ogretir, I. G. Csizmadia), Kluwer Academic, The Netherlands, **1991**, p. 167.
[42] S. Miertus, E. Scrocco, J. Tomasi, *Chem. Phys.* **1981**, *55*, 117.
[43] S. Miertus, J. Tomasi, *Chem. Phys.* **1982**, *65*, 239.
[44] M. Cossi, V. Barone, R. Commi, J. Tomasi, *Chem. Phys. Lett.* **1996**, *255*, 327.
[45] V. Barone, M. Cossi, B. Menucci, J. Tomasi, *J. Chem. Phys.* **1997**, *107*, 3210.
[46] P. E. M. Siegbahn, M. R. A. Blomberg, *Chem. Rev.* **2000**, *100*, 421.
[47] L. Noodleman, T. Lovell, W. G. Han, J. Li, F. Himo, *Chem. Rev.* **2004**, *104*, 459.
[48] F. Maseras, K. Morokuma, *J. Comput. Chem.* **1995**, *16*, 1170.
[49] S. Humbel, S. Sieber, K. Morokuma, *J. Chem. Phys.* **1996**, *105*, 1959.
[50] T. Matsubara, S. Sieber, K. Morokuma, *Int. J. Quantum Chem.* **1996**, *60*, 1101.
[51] M. Svensson, S. Humbel, R. D. J. Froese, T. Matsubara, S. Sieber, K. Morokuma, *J. Phys. Chem.* **1996**, *100*, 19357.
[52] M. Svensson, S. Humbel, K. Morokuma, *J. Chem. Phys.* **1996**, *105*, 3654.
[53] S. Dapprich, I. Komáromi, K. S. Byun, K. Morokuma, M. J. Frisch, *J. Mol. Struct.* **1999**, *462*, 1.
[54] T. Vreven, K. Morokuma, *J. Comput. Chem.* **2000**, *21*, 1419.
[55] M. Torrent, T. Vreven, D. G. Musaev, K. Morokuma, O. Farkas, H. B. Schlegel, *J. Am. Chem. Soc.* **2002**, *124*, 192.
[56] A. K. Rappé, C. J. Casewit, K. S. Colwell, W. A. Goddard III, W. M. Skiff, *J. Am. Chem. Soc.* **1992**, *114*, 10024.
[57] T. A. Wesolowski, A. Warshel, *J. Phys. Chem.* **1993**, *97*, 8050.
[58] G. Hong, M. Strajbl, T. A. Wesolowski, A. Warshel, *J. Comput. Chem.* **2000**, *21*, 1554.
[59] J. Åqvist, A. Warshel, *Chem. Rev.* **1993**, *93*, 2523.
[60] W. Kohn, L. J. Sham, *Phys. Rev.* **1965**, *140*, A1133.
[61] T. A. Wesolowski, *J. Chem. Phys.* **1997**, *106*, 8516.
[62] A. Lembarki, H. Chermette, *Phys. Rev. A* **1994**, *50*, 5328.
[63] M. Dulak, T. A. Wesolowski, *Int. J. Quantum Chem.* **2005**, *101*, 543.
[64] A. M. Koester, R. Flores-Moreno, G. Geudtner, A. Goursot, T. Heine, J. U. Reveles, A. Vela, D. R. Salahub, deMon **2003**, NRC, Canada.
[65] N. Godbout, D. R. Salahub, J. Andzelm, E. Wimmer, *Can. J. Chem.* **1992**, *70*, 560.
[66] A. M. Köster, P. Calaminici, S. Escalante, R. Flores-Moreno, A. Goursot, S. Patchkovskii, J. U. Reveles, D. R. Salahub, A. Vela, T. Heine, The deMon User's Guide, Version 1.0.3, **2003–2004**.
[67] J. H. Enemark, J. J. A. Cooney, J. J. Wang, R. H. Holm, *Chem. Rev.* **2004**, *104*, 1175.
[68] J. J. Wang, O. P. Kryatova, E. V. Rybak-Akimova, R. H. Holm, *Inorg. Chem.* **2004**, *43*, 8092.
[69] C. A. McDevitt, G. R. Hanson, C. J. Noble, M. R. Cheesman, A. G. McEwan, *Biochemistry* **2002**, *41*, 15234.
[70] T. Waters, X.-B. Wang, X. Yang, L. Zhang, R. A. J. O'Hair, L.-S. Wang, A. G. Wedd, *J. Am. Chem. Soc.* **2004**, *126*, 5119.
[71] M. Kaupp, *Angew. Chem.* **2004**, *116*, 554; *Angew. Chem. Int. Ed.* **2004**, *43*, 546.
[72] F. Hasanayn, M.-Z. Markarian, R. Al-Rifai, *Inorg. Chem.* **2004**, *43*, 3691.
[73] M. Porembski, J. C. Weisshaar, *J. Phys. Chem. A* **2001**, *105*, 4851.
[74] B. S. Jursic, *J. Mol. Struct.* **1998**, *430*, 17.
[75] P. Nachtigall, K. D. Jordan, A. Smith, H. Jonsson, *J. Chem. Phys.* **1996**, *104*, 148.

Received: July 9, 2005
Revised: October 27, 2005
Published online: January 13, 2006

